Cryo-ET reveals nucleosome reorganization in condensed mitotic chromosomes *in vivo*

Shujun Cai, Chen Chen, Zhi Yang Tan, Jian Shi, and Lu Gan*

Department of Biological Sciences and Centre for BioImaging Sciences, National University of Singapore, Singapore 117543

* Correspondence: lu@anaphase.org

SUMMARY

At the onset of mitosis, chromosomes condense into discrete bodies. This transformation involves rearrangement at the nucleosome level and has consequences for transcription, but the details remain unclear. Here, we use cryo-electron tomography to determine the 3-D arrangement of nucleosomes and other large nuclear features in interphase and mitotic fission yeast cells. Nucleosomes can form heterogenous clusters in both interphase and mitotic cells, but none the size of a Hi-C domain. Furthermore, the nucleosomes are mingled with two features: nucleosome-free pockets and ribosome-sized “megacomplexes”. Compared to interphase chromatin, the nucleosomes in mitotic chromatin pack in larger clusters. Furthermore, mitotic chromatin contained fewer megacomplexes. However, nearest-neighbor distance analysis revealed that mitotic nucleosome clusters have the same packing density as in interphase. Therefore, the uneven chromosome condensation helps explain a longstanding enigma of mitosis: most genes are silenced but a subset is upregulated.

INTRODUCTION

Chromatin structure influences key nuclear activities such as transcription and replication (Dixon et al., 2016). The fundamental unit of chromatin is the nucleosome, which consists of ~147 bp of DNA wrapped around a histone octamer (Luger et al., 1997). In mammalian cells, 2 - 35 nucleosomes pack into heterogeneous “clutches” (Ricci et al., 2015) and more than 500 nucleosomes associate as topologically associating domains (Dixon et al., 2012). Likewise, in the fission yeast *Schizosaccharomyces pombe*, between 300 - 700 nucleosomes associate as compact globular chromatin bodies called globules (Mizuguchi et al., 2014). These studies suggest that chromatin higher-order structure arises from physical interactions of large groups of nucleosomes.

In mitotic cells, chromosomes condense into discrete chromatids. The factors involved in condensation have been well characterized (Hirano, 2016) and a number of models have been proposed for the large-scale organization of chromatin domains (Maeshima and Eltsov, 2008). However, the molecular details of chromatin reorganisation are still unknown. Knowledge of how chromatin condenses in 3-D at the single-nucleosomes level is needed to explain the nearly global mitotic transcriptional repression observed in many eukaryotes (Struhl, 1998). Likewise, a 3-D model of chromatin could also explain how a subset of genes escape this mitotic repression and get upregulated (Rustici et al., 2004; Oliva et al., 2005; Peng et al., 2005).

Some insights on *in vivo* chromatin organisation were made possible by new methods, including chromatin-conformation capture (Hi-C), super-resolution microscopy, and traditional EM of cells stained with DNA-proximal osmium (Beliveau et

al., 2015; Pombo and Dillon, 2015; Ou et al., 2017). However, the resultant models are limited because these methods rely on population-averaged data, or have low resolution, or perturb the sample due to the fixation, dehydration and staining perturbations, respectively. Electron cryotomography (cryo-ET) complements these approaches because it enables direct visualization of macromolecular complexes in a life-like frozen-hydrated state inside cells in 3-D at ~ 4-nm resolution (Gan et al., 2013). Being a label-free method, cryo-ET image features arise from the molecules themselves, revealing the positions of all macromolecular complexes in a cell. Using cryo-ET, we previously showed that nucleosomes in picoplankton and budding yeast pack irregularly, but we also found that the chromosomes in these cells did not compact into discrete chromatids (Gan et al., 2013; Chen et al., 2016).

We have now used cryo-ET to directly visualize the mitotically rearranged chromatin *in vivo* in the fission yeasts *S. pombe* and *S. japonicus*. To obtain cryotomograms with sufficient contrast to resolve nucleosomes, we imaged cells that were thinned by cryomicrotomy. To better understand the heterogeneous complexes in the crowded nucleoplasm, we took advantage of recent advances in phase-contrast hardware and 3-D classification software (Bharat and Scheres, 2016; Khoshouei et al., 2017). We found that in interphase, nucleosomes frequently associate as small clusters or short chains. Nucleosome-free pockets and megadalton-sized “megacomplexes” are interspersed among these nucleosome clusters. In mitosis, chromosomes condense unevenly and have slightly larger nucleosome clusters. Mitotic chromosomes also have nucleosome-free pockets, but fewer megacomplexes. These phenotypes are conserved

73 in both yeasts and lead to a model that explains how mitotic chromatin is permissive to

74 some genes but repressive to most others.

RESULTS

S. pombe subcellular structures are revealed at molecular resolution by cryo-ET

To understand how native chromatin organization differs between interphase and mitosis, we imaged *S. pombe* cells by cryo-ET of frozen-hydrated sections (cryosections, ~ 90 - 130 nm nominal thickness). Because it is challenging to determine the cell-cycle stage using the cryo-EM image alone, we arrested temperature-sensitive *cdc25-22* cells in G2 phase (Fantes, 1979) and cold-sensitive *nda3-KM311* cells in prometaphase (Hiraoka et al., 1984). Fluorescence microscopy confirmed that the latter cells have the well-known mitotic chromosome-condensation phenotype (Fig. 1A).

In a typical cryotomogram of an *S. pombe* cell, we could recognize organelles by their size and membrane morphology. Prominent organelles included the endoplasmic reticulum, vesicles, and the nucleus (Fig. 1B and C). To further assess the quality of the cryosections and data, we performed subtomogram averaging of cytoplasmic ribosomes (Fig. S1A, B). The resulting average was similar to a low-pass-filtered budding-yeast ribosome crystal structure (Fig. S1C) (Ben-Shem et al., 2011). Therefore, the conformation of large complexes are preserved at the molecular level.

Interphase chromatin is arranged as loosely packed nucleosomes and heterogeneous nucleosome clusters

G2-phase cell nuclei are filled with many nucleosome-like granular densities, which, for the sake of brevity, herein we call nucleosomes for brevity due to their size, shape, abundance, location, and condensation phenotype all being consistent with nucleosomes (see below). Nucleosomes frequently associate as small heterogeneous

clusters less than 50-nm wide (Fig. 2B). Chain-like nucleosome configurations are also abundant (Fig. 2C). The remaining nucleosomes are not clustered together (Fig. 2D). Efforts to automatically identify clusters of nucleosomes did not produce clusters with distinct motifs due to their heterogeneous positions. Small nucleosome-free "pockets" (< 50 nm) are also abundant (Fig. 2E). Densities much larger than nucleosomes (> 20 nm) are spread throughout the nucleus (Fig. 2F). These densities are consistent with being multi-megadalton nuclear assemblies such as pre-ribosomes, spliceosomes, and transcription preinitiation complexes (Gleizes et al., 2001; Allen and Taatjes, 2015; Oesterreich et al., 2016); we call these "megacomplexes" for brevity. Therefore, in interphase, nucleosomes associate into many heterogeneous small clusters, interspersed among pockets and megacomplexes.

Condensed mitotic chromosomes contain fewer megacomplexes

Unlike in G2-phase cells, in each cryotomogram of a prometaphase cell we found a single position that has many features consistent with its being a section through a condensed chromosome. For example, nucleosomes-like densities are abundant within these positions, but much rarer outside (Fig. 3A-C). Compared to G2-phase cells, in which abundant megacomplexes are interspersed with the chromatin (Fig. 2A), megacomplexes are mostly absent from these large contiguous regions in prometaphase cells (Fig. 3A). These positions are hundreds of nanometers wide, matching the size of condensed chromosomes seen by fluorescence microscopy (Fig. 1A, S2). If these positions are indeed chromosomes, there should be a large contiguous volume in the cell with few megacomplexes. To test this hypothesis, we sampled a

larger nuclear volume by cryo-ET of 5 nearly sequential cryosections (summing to ~ 700 nm thick) of the same cell (Fig. S3A). We saw a single megacomplex-poor region in each of these cryosections, which is consistent with these positions being sections through one or two of the three fission-yeast chromosomes (Fig. S3B-F). Taken together, we located mitotic chromosomes and found they have fewer megacomplexes within.

Nucleosome clusters and loosely packed nucleosomes also coexist within mitotic condensed chromosomes

In conventional (defocus) cryotomograms, we noticed that most nucleosomes appear more densely packed in prometaphase cells (Fig. S4). To better understand how chromatin is organized, we imaged cells by Volta phase contrast cryo-ET (Fig. S5). Volta cryo-EM data have much more contrast, making it possible to locate and determine the orientations of smaller protein complexes and to resolve protein complexes packed to near-crystalline density inside of cells (Engel et al., 2015; Khoshouei et al., 2017). The Volta data confirmed what we learned from defocus cryo-ET: nucleosomes more frequently packed into larger clusters in prometaphase cells than in the G2-phase cells, but the boundary of clusters is less clear (Figs. 4A and B, S5). Importantly, we also observed some loosely packed nucleosomes in prometaphase cells (Figs. 4C and S5B, D), meaning that condensation is uneven. In summary, mitotic chromosomes consist of both densely and loosely packed nucleosomes.

The existence of loosely packed prometaphase nucleosomes suggests that mitotic chromatin is permissive to transcriptional machines, which is supported by the

observation that some genes are up-regulated during mitosis (Rustici et al., 2004; Oliva et al., 2005; Peng et al., 2005). However, these earlier studies could not determine if mitotic cells are undergoing active RNA polymerase II transcription or if they simply have stable mRNAs leftover from G2 phase. Phosphorylation of RNA polymerase II at Serine 2 of the carboxy-terminal domain (CTD) heptamer repeat is a conserved marker of transcription elongation (Komarnitsky et al., 2000; Harlen and Churchman, 2017). Using immunofluorescence, we confirmed the existence of RNA polymerase II with phospho-Ser2 CTD, and therefore active transcription, in prometaphase chromosomes (Fig. S6). To rule out the possibility of abnormal transcriptional activity in the mutants, we also performed this experiment in asynchronous wild type cells. We also detected phospho-Ser2 CTD signal in early mitotic cells. Therefore, transcription is not shut-down globally in mitotic *S. pombe* cells.

To analyse the nucleosome rearrangement more objectively, we performed template matching to find their 3-D positions in Volta cryotomograms. This analysis showed that nucleosome formed clusters in both G2-phase and prometaphase cells, but appear more crowded in the latter (Fig. 5A, B). If chromosomes condense via a uniform accretion of all nucleosomes, the average nucleosome nearest-neighbor distance (NND) distribution should shorten. However, the NND distributions of nucleosome hits in G2-phase and prometaphase cells were indistinguishable (two-tailed t-test, $p > 0.05$) (Fig. 5C). While mitotic chromatin might not condense by compaction of nearest-neighbor nucleosomes, they might condense from changes in interactions between groups of nucleosomes. We tested this hypothesis by creating histograms of 10^{th} NNDs and found that the population shifted to shorter distances in prometaphase cells (two-

tailed t-test, $p < 0.001$) (Fig. 5D), which explains the more-crowded appearance of prometaphase nucleosomes. Taken together, our analyses reveal that chromosomes condense by the merging of small nucleosome clusters, resulting in a closer association between distant nucleosomes (Fig. 5E, F).

As an alternative approach to studying nucleosomes *in vivo*, we performed cryo-ET on the undigested chromatin from lysates of G2-phase and prometaphase *S. pombe* cells. Cryotomograms of cell lysis products can reveal more clearly the positions of nucleosomes (Cai et al., 2017). Subtomogram averages of nucleosome template-matching hits revealed unambiguous features of mono-nucleosomes including the groove between two DNA gyres (Fig. S7), demonstrating that our template-matching approach can pick out most nucleosomes. In the lysates, there are many large nucleosome-free pockets wider than 50 nm in G2-phase chromatin. In contrast, prometaphase chromatin remained as compact bodies with only a few smaller pockets (Fig. S8). Therefore, consistent with our *in vivo* results, prometaphase chromatin also has denser nucleosome packing *in vitro* (Fig. S8).

S. japonicus **and** ***S. pombe*** **chromosomes condense by similar means**

To test whether the formation of larger nucleosome clusters during condensation is conserved, we imaged *S. japonicus*, a bigger fission yeast that also undergoes mitotic condensation (Robinow and Hyams, 1989). *S. japonicus* has the same genome size (~ 12Mb) as *S. pombe*, but has a nucleus at least 8-fold more voluminous. Because *S. japonicus* is a less-developed model organism, we used asynchronous wild-type cells. These cells were frozen, cryosectioned, and subjected to Volta cryo-ET just like for *S.*

190 *pombe*. We used microtubules as cytological markers because a previous study
191 showed that cells that have cytoplasmic microtubules are in interphase, whereas cells
192 that have nuclear microtubules are in mitosis (Yam et al., 2013). We found densely
193 packed nucleosomes in *S. japonicus* mitotic chromosomes (Fig. S9A-D). Furthermore,
194 NND and 10^{th}-NND analyses show that the nucleosome NND distributions were similar
195 in interphase and mitosis (two-tailed t-test, $p > 0.05$) , but that the 10^{th}-NND distribution
196 was shorter in mitosis (two-tailed t-test, $p < 0.001$) (Fig. S9E, F). Therefore, the
197 formation of larger and closer nucleosome clusters in mitosis is a conserved phenotype
198 in fission yeasts.
199
200 **Nucleosomes do not packed in a fixed motif**
201 Our previous study on natural *S. cerevisiae* chromatin *in vitro* showed that pairs of
202 nucleosomes sometimes packed face-to-face (Cai et al., 2017), which can limit access
203 to histone motifs like the acidic patch (Luger et al., 1997). However, our 2-D
204 classification of di-nucleosomes in *S. pombe* did not reveal any classes containing face-
205 to-face-packed nucleosomes (Fig. S11), meaning that such nucleosome-nucleosome
206 interactions must be extremely rare. Instead, di-nucleosomes were packed irregularly,
207 including edge-to-edge packing, with ~ 3-nm gaps in between. Compared with
208 prometaphase cells (Fig S11B and D), we noticed that G2-phase nucleosomes were
209 more heterogeneously packed (Fig. S11A and C). Taken together, our 2-D classification
210 analyses reveal irregular packing of nucleosomes *in vivo*.
211

A subset of nucleosomes may be partially unwrapped

In a rare instances, we were able to resolve densities that resemble linker DNA spanning two nucleosome-like densities in *S. pombe* G2-phase chromatin (Fig. S10A, B). Many of these linker-DNA-like densities were much longer than the average ~ 2 nm expected from MNase-digestion experiments (Fig. S10A-D) and nucleosome-mapping studies (Lantermann et al., 2010). Furthermore, in the NND analysis, there are a large number of nucleosome pairs that have NND values greater than 12 nm, i.e., the gap between two adjacent nucleosomes are larger than 2 nm (Fig. 5C). One explanation is that the larger separation reflects the high end of the distribution of linker DNA lengths. Alternatively, some nucleosomes might be partially unwrapped – such as may be expected of fragile or prenucleosomes (Fei et al., 2015; Kubik et al., 2015), resulting in apparently longer linker DNA (Fig. S10E, F). The possibility of partially unwrapped nucleosomes led us to test whether the nucleosomes *in vivo* resembled mononucleosomes. To do this, we performed 2-D and 3-D classification of nucleosome template-matching hits (Bharat and Scheres, 2016). Although 3-D class averages have the correct size of nucleosomes, none of them resemble the low-pass-filtered crystal structure of the mono-nucleosome (Fig. S12) (Luger et al., 1997). This difference might be due to either the insufficient signal-to-noise ratio of our dataset or high heterogeneity of nucleosome densities.

DISCUSSION

We have directly visualized chromatin in both interphase and mitotic fission-yeast cells by cryo-ET. Nucleosomes associate into small heterogeneous clusters in interphase. Mitotic cells have larger nucleosome clusters, but the nearest-neighbor distance does not shorten. Condensed chromosomes also contain fewer megacomplexes. Following cell lysis, mitotic chromatin remains more compact than interphase chromatin, suggesting that mitotic chromatin has properties that make it inherently prone to self-association. Classification analysis suggests that contrary to universal depictions in the literature, most nucleosomes *in vivo* are conformationally heterogeneous or bound by nucleosome-associated proteins, or both. We propose a model of chromosome condensation at the nucleosome level (Fig. 6). In uncondensed chromosomes, nucleosomes are loosely packed as small and heterogenous clusters. Upon mitotic condensation, a subset of nucleosomes become part of large clusters. As a result of this chromatin reorganization, megacomplexes become mostly absent from the chromatin.

A recent electron tomography study (ChromEMT) showed that mammalian chromatin could be better visualized when treated with a DNA-binding dye that generates a local cloud of osmiophilic polymers (Ou et al., 2017). In that study, the cells were processed by traditional EM methods, meaning that recorded densities were from osmium deposits in a cell that had been subjected to dehydration, multiple rounds of chemical fixation, and plastic embedment. Assuming that the osmium stain distribution remained localized within a few nanometers of the original nucleosome positions, the study concluded that mammalian chromatin is best explained by a beads-on-a-string configuration, and that chromosomes condense by these beads folding back upon

254 themselves. Unlike our study, the ChromEMT study did not report any clusters of
255 nucleosomes or any megacomplexes. Instead, the space in between the stained
256 positions appeared like large voids.
257
258 **Cryo-ET reveals new insights into higher-order chromatin organisation**
259 Our cryotomograms of G2 phase *S. pombe* reveal that at the single-cell level, there are
260 many small heterogenous clusters (Fig. 2D). However, most clusters are smaller than
261 the globules inferred from Hi-C experiments (Mizuguchi et al., 2014). This inconsistency
262 between single-cell and population studies has been reported before -- single-cell Hi-C
263 studies showed smaller or more disperse chromatin bodies than conventional
264 (population based) Hi-C studies (Nagano et al., 2013; Flyamer et al., 2017; Nagano et
265 al., 2017). In light of our direct observation of nucleosome clusters, this difference can
266 be reconciled as follows. Each cell has different sets of small nucleosome clusters,
267 probably as a consequence of chromatin dynamics (Nozaki et al., 2017). A large
268 population of cells, each with a smaller cluster of nucleosomes at a given locus, could
269 produce the larger globule if their Hi-C signals were summed (Fig. S13). Therefore,
270 small heterogenous nucleosome clusters are the primary higher-order structure of
271 chromatin in fission yeast.
272 In higher eukaryotes, nucleosome arrays are also thought to fold into chromatin
273 loops, which in human cells can bring together loci that are separated by up to 2 Mb that
274 correspond to ~10,000 nucleosomes (Rao et al., 2014). Hi-C did not reveal any loops in
275 *S. pombe* (Mizuguchi et al., 2014), but we do see curved nucleosome chains, which
276 might be portions of short loops (Fig. 2C). If these chains were indeed portions of loops,

277 their loop-like Hi-C signature (off-axis peaks) could have been lost due to the
278 aforementioned population averaging effect or due to insufficient Hi-C resolution. It is
279 unknown if short chromatin loops adopt a "Ω" shape or if they are irregular. Such a
280 question may eventually be addressable once imaging technology improves to a point
281 where the majority of linker DNAs connecting sequential nucleosomes can be resolved
282 in frozen-hydrated cells.
283
284 **The role of uneven condensation in transcriptional regulation**
285 It has long been known that there is a strong correlation between chromosome
286 condensation and transcriptional repression (Taylor, 1960; Prescott and Bender, 1962).
287 Mechanistic evidence of mitotic repression came from the observation that mitotic
288 condensation is coincident with transcription-factor displacement (Martinez-Balbas et
289 al., 1995). In fission yeast, there is an overall transcriptional repression in mitosis (Oliva
290 et al., 2005), but many cell-cycle related genes actually get upregulated during mitosis
291 (Rustici et al., 2004; Oliva et al., 2005; Peng et al., 2005). In agreement, our
292 immunofluorescence images detected elongating RNA polymerase II in mitotic *S.*
293 *pombe* chromosomes. How could such an enigma be explained? Our study shows that
294 most nucleosomes in mitotic chromosomes do not pack face-to-face, which enables
295 access to a subset of protein complexes that interact with this nucleosome interphase
296 (McGinty and Tan, 2015). Mitotic fission yeast nucleosomes are nevertheless densely
297 packed and generally non-permissive to megacomplexes, including large transcription
298 machines. However, we find that condensation is uneven because there are a few
299 nucleosome-free positions in between nucleosome clusters (Figs. 4C, S5D). These

positions would remain permissive to either the passage or assembly of transcription megacomplexes such as spliceosomes and transcription preinitiation complexes. Indeed, a few other nucleosome-free positions in mitotic chromatin contain megacomplexes, but it remains to be determined whether these were pre-formed complexes that diffused into an already-condensed chromosome or if they assembled *de novo*. We favor this latter possibility because the subunits of megacomplexes, which are much smaller, can pass between the nucleosomes due to transient opening of chromatin from thermal motions (Hihara et al., 2012). Uneven condensation therefore offers a molecular explanation for the fine-grained control of mitotic transcription.

METERIALS AND METHODS

Cell culture

S. pombe cell culture (Forsburg, 2003), G2-phase arrest (Ducommun et al., 1990) and prometaphase arrest (Hiraoka et al., 1984) were performed as previously reported. *nda3-km311* cells were incubated overnight in yeast-extract supplemented (YES) medium (30 g/L glucose, 5 g/L yeast extract, 225 mg/L adenine, 225 mg/L histidine, 225 mg/L leucine, 225 mg/L uracil) at 30°C with shaking. When the optical density at 600 nm (OD_{600}) reached ~0.2, the cultures were cooled by incubation in a 20°C shaker. After incubation with shaking for 10 hr at this lower temperature, above 90% of cells were arrested in a prometaphase state. *cdc25-22* cells were incubated in YES medium at 25°C with shaking overnight. When the OD_{600} reached ~0.2, the cultures were warmed to a 36°C in a water bath and then transferred to a 36°C shaker. After 4 hr, the majority of cells were arrested at G2 phase. *S. japonicus* cells were cultured in YES medium at 30°C with shaking overnight until cells reached mid-log phase (OD_{600} = ~0.6) (Yam et al., 2013).

Fluorescence microscopy

Cells were stained with DAPI following a published protocol (Toda et al., 1981). Cells (1 ml) were fixed with 2.5% formaldehyde for 60 mins at the restrictive temperature for mutants. The cells were washed twice by centrifugation at 1500 *x g* for 1 min and resuspension with distilled water. They were pelleted at 1500 *x g* for 1 min and stained by resuspension in 50 µl PBS, pH 7.4, containing 1 µg/ml DAPI. Ten µl of the sample was then added to the slide and imaged using a PerkinElmer Ultraview Vox Spinning Disc confocal microscope (PerkinElmer, Waltham, MA). Images were recorded using an 100x oil-immersion objective.

Immunofluorescence

Log-phase cells (~10 ml) were fixed with 3.7% formaldehyde for 90 min at 30°C (or the restrictive temperature for mutants). Cells were collected by centrifugation at 1500 *x g* for 5 min. Cells were then resuspended in 1 ml PEM buffer (0.1 M PIPES pH 6.95, 2 mM EGTA, 1 mM $MgSO_4$). Cells were washed once with 1 ml PEM this way and then resuspended in 1ml PEMS (1.2 M sorbitol in PEM). Next, cells were spheroplasted for 15 minutes by incubation with lysis-enzyme cocktail, diluted 1:1000 in PEMS at 30°C. Cells were washed with PEMS. The pellet was then resuspended in PEMS with 1% Triton X-100 and incubated at 22°C for 5 min. Cells were then washed twice with PEM and incubated in PEMBAL (PEM, 1% BSA, 100 mM L-Lysine hydrochloride) at 22 °C for 1 hour. Cells were then incubated with rabbit anti-RNA polymerase II CTD repeat YSPTSPS (phospho S2) antibody in PEMBAL (1:1000 dilution) at 22 ºC for 1 hour. Cells were washed three times with 1 ml PEMBAL and then incubated with Alexa Fluor 488-coupled donkey anti-rabbit antibodies at 22 ºC for 1 hour. Cells were then washed three times with PEM and resuspended in 50 µl 1 µg/ml DAPI.

Self-pressurized freezing

Self-pressurized freezing was performed based on a previous method, with modifications (Yakovlev and Downing, 2011). *S. pombe* were grown in YES medium until the OD_{600} reached 0.2 - 0.6. Cells were pelleted by centrifuging at 1500 *x g* for 5 min. Dextran (40 kDa) was added to the cell pellet as an extracellular cryoprotectant to a final concentration of 30%. The cells were then quick-spun to remove bubbles and then loaded into a copper tube (0.45 / 0.3 mm outer / inner diameters) with a syringe-type filler device (Part 733-1, Engineering Office M. Wohlwend GmbH). The tube was sealed by crimping both ends with flat jaw pliers. The sealed tube was held horizontally 3 cm above the liquid-ethane cryogen surface, and then dropped into

358 the cryogen. The flattened ends of the tube were then cut off with a specially designed guillotine
359 under liquid nitrogen.
360
361 **Vitreous sectioning**
362 Vitreous sectioning was performed as previously described with modifications (Chen et al.,
363 2016). A perforated-carbon grid or continuous carbon grid was coated with 10 nm gold colloids
364 as fiducials for cryotomographic alignment. Gold solution (5 µl at 5.7 x 10^{12} particles/ml) in 0.1
365 mg/ml BSA was applied to the grid and then air-dried. Frozen-hydrated cells were cut into a 70-
366 nm thick cryo-ribbon using a 35° diamond knife (Cryo35, Diatome, Nidau, Switzerland) in a
367 Leica UC7/FC7 cryo-ultramicrotome (Leica Microsystems, Vienna, Austria) at -150°C. Once the
368 ribbon was ~3 mm long, the colloidal-gold-coated EM grid was placed underneath the ribbon.
369 To minimize occlusion by grid bars at high tilt during cryotomographic imaging, the grid as
370 aligned so that the ribbon was parallel with and in between the grid bars. The ribbon was then
371 attached to the grid by operating the Crion in “charge” mode for ~30 seconds. The grid was
372 stored in liquid nitrogen until imaging.
373
374 **Cell lysis**
375 Log-phase *S. pombe* cells were collected by centrifuging at 1500 *x g* for 5 min and then
376 spheroplasted for 15 minutes by incubation with lysis-enzyme cocktail at either 30°C or the
377 restrictive temperature for mutants. The spheroplasts were pelleted at 1500 *x g* for 2 mins at 22
378 °C and then lysed in 20 µl lysis buffer (50 mM EDTA and a 1:1000 dilution of protease inhibitor
379 cocktail) on ice for 15 min.
380
381 **Plunge freezing**
382 Plunge freezing was done using a Vitrobot Mk IV (Thermo, Waltham, MA) operated at 4°C with
383 80% humidity. *S. pombe* cell lysates (4 µl) were applied to a freshly glow-discharged perforated-

carbon grid. The grid was blotted once (blot force:1, blot time: 3s) with filter paper and then plunged into liquid ethane.

Electron cryotomography

Tilt series were collected using FEI TOMO4 on a Titan Krios cryo-TEM (Thermo, Waltham, MA) operated at 300 KeV and equipped with a field-emission gun, a Volta phase-plate device, and a Falcon II direct-detection camera. Details of the imaging parameters are shown in Table S1. Image alignment, CTF correction, low-pass filtration, 3-D reconstruction were done using the IMOD software package. Note that Volta cryotomograms were not CTF corrected. Cryotomograms were visualized as tomographic slices with 3dmod and as isosurfaces with UCSF Chimera.

Template matching

Template matching was done using PEET. A manually-selected subtomogram containing a nucleosome-like particle served as a template. This template was multiplied with a spherical mask to suppress the influence of background nucleoplasmic densities. The search grid with a 10-nm spacing was generated within the nucleus. Hits within 6 nm were considered as duplicates and the extra hit was automatically removed. The criteria of cross-correlation coefficient cutoff were the same as in our previous report (Cai et al., 2017). Briefly, we first used the average of cross-correlation coefficients of all template-matching hits as a cutoff. We then manually inspected the hits in the tomogram and adjusted the cutoff (if needed) to minimize the number of detectable false positives and false negatives. To further remove false positives from megacomplexes, another round of template matching was performed using a ribosome-like density as a template. The nucleosome hits that were within 12.5 nm of these megacomplexes were then removed with a Matlab script (available upon request; Mathworks, Natick, MA).

For dinucleosome template matching, a manually-selected subtomogram of a di-nucleosome served as a template. This template was multiplied with a cylindrical mask (diameter: 15 nm, height: 22 nm) rotated to align with the longitudinal axis of the dinucleosome template. The search grid with a 25-nm spacing was generated within the chromatin. Due to missing wedge artifact, nucleosomes have higher resolution in X-Y. Therefore, the angular search around the X and Y axes was disabled. Hits within 15 nm were considered as duplicates. The criteria of cross-correlation coefficient cutoff were the same as the one described above for mononucleosomes. False positives from megacomplexes fell into their own classes in the subsequent 2-D classification (see below) and were removed at that point.

2-D and 3-D classification

Subtomogram classification and 3-D averaging of nucleosomes were done in RELION 1.4 and RELION 2.0, following the workflow of our previous study (Cai et al., 2017). The 3-D coordinates of template-matching hits were imported into RELION with a 15.6 nm box size and 13.5 nm mask diameter. For 2-D classification, the number of classes was set to 50 and the resolution of the data was limited to 3 nm. All nucleosome-like classes were selected. For 3-D classification, the number of classes was set to between 10 and 20, and the resolution limit was set to 2 nm. Two to three rounds of 3-D classification were performed, with false positive removal in between rounds.

For di-nucleosome 2-D classification, the box size and the mask diameter were set to 30 nm and 26 nm, respectively. As a default setting, RELION produce projections of all densities within the boxes, including the nucleoplasmic densities above and below dinucleosomes. To only include densities of dinucleosomes, a python script (available upon request) was used to generate projections from thinner boxes (height: 17.5 nm). The resolution of the data was limited to 2 nm to suppress the effects of high-resolution noise. The number of classes was set to 100, but many of the classes were very similar and therefore merged.

435

436 **Nearest-neighbor distance analysis**

437 Nearest-neighbor distance analysis of template-matching hits (Figs. 5 and S9) was performed
438 as previously described (Cai et al., 2017). The coordinates of the nucleosome hits were
439 imported into Matlab. NND and 10^{th} NND were calculated using the Matlab function
440 nearestneighbour.m. The script is available upon request.

441

442 **Two-tailed t-test**

443 Two-tailed t-tests for NND values were performed in Excel using TTEST function. The number
444 of NND values analysed for G2-phase and prometaphase *S. pombe*, interphase and mitotic *S.*
445 *japonicus* were 10292, 11835, 9397, 4474, respectively.

446

447 **Data sharing**

448 A cryotomogram, corresponding to Fig. 1, was deposited in the EMDataBank as EMD-####.
449 The tilt series for all cryotomograms presented in this manuscript were deposited in the Electron
450 Microscopy Public Image Archive as EMPIAR-####.

Acknowledgements

We thank the CBIS microscopy staff for support and training. We thank Mohan Balasubramanian and Yinyi Huang for providing *S. pombe* strains and advice on *S. pombe* culture. We thank Snezhka Oliferenko for advice on *S. japonicus* culture and manuscript feedback. *S. japonicus* strains were obtained from JapoNet. SC, CC, ZYT and LG were supported by NUS startups R-154-000-515-133, R-154-000-524-651, and D-E12-303-154-217, R-154-000-558-133, and MOE T2 R-154-000-624-112.

Contributions

S.C - experiments, project design, writing, CC - training, ZT - experiments, JS - training, LG - project design, writing.

463 **REFERENCES**

464 Allen, B.L., and Taatjes, D.J. (2015). The Mediator complex: a central integrator of transcription.
465 Nature reviews Molecular cell biology *16*, 155-166.

466 Beliveau, B.J., Boettiger, A.N., Avendano, M.S., Jungmann, R., McCole, R.B., Joyce, E.F., Kim-
467 Kiselak, C., Bantignies, F., Fonseka, C.Y., Erceg, J.*, et al.* (2015). Single-molecule super-
468 resolution imaging of chromosomes and in situ haplotype visualization using Oligopaint FISH
469 probes. Nature communications *6*, 7147.

470 Ben-Shem, A., Garreau de Loubresse, N., Melnikov, S., Jenner, L., Yusupova, G., and
471 Yusupov, M. (2011). The structure of the eukaryotic ribosome at 3.0 A resolution. Science *334*,
472 1524-1529.

473 Bharat, T.A., and Scheres, S.H. (2016). Resolving macromolecular structures from electron
474 cryo-tomography data using subtomogram averaging in RELION. Nat Protoc *11*, 2054-2065.

475 Cai, S., Song, Y., Chen, C., Shi, J., and Gan, L. (2017). Natural Chromatin Is Heterogeneous
476 And Self Associates In Vitro. bioRxiv, 139543.

477 Chen, C., Lim, H.H., Shi, J., Tamura, S., Maeshima, K., Surana, U., and Gan, L. (2016).
478 Budding yeast chromatin is dispersed in a crowded nucleoplasm in vivo. Molecular biology of
479 the cell *27*, 3357-3368.

480 Dixon, J.R., Gorkin, D.U., and Ren, B. (2016). Chromatin Domains: The Unit of Chromosome
481 Organization. Molecular cell *62*, 668-680.

482 Dixon, J.R., Selvaraj, S., Yue, F., Kim, A., Li, Y., Shen, Y., Hu, M., Liu, J.S., and Ren, B. (2012).
483 Topological domains in mammalian genomes identified by analysis of chromatin interactions.
484 Nature *485*, 376-380.

485 Ducommun, B., Draetta, G., Young, P., and Beach, D. (1990). Fission yeast cdc25 is a cell-
486 cycle regulated protein. Biochemical and biophysical research communications *167*, 301-309.

487 Engel, B.D., Schaffer, M., Kuhn Cuellar, L., Villa, E., Plitzko, J.M., and Baumeister, W. (2015).
488 Native architecture of the Chlamydomonas chloroplast revealed by in situ cryo-electron
489 tomography. Elife *4*.

490 Fantes, P. (1979). Epistatic gene interactions in the control of division in fission yeast. Nature
491 *279*, 428-430.

492 Fei, J., Torigoe, S.E., Brown, C.R., Khuong, M.T., Kassavetis, G.A., Boeger, H., and Kadonaga,
493 J.T. (2015). The prenucleosome, a stable conformational isomer of the nucleosome. Genes &
494 development *29*, 2563-2575.

495 Flyamer, I.M., Gassler, J., Imakaev, M., Brandao, H.B., Ulianov, S.V., Abdennur, N., Razin,
496 S.V., Mirny, L.A., and Tachibana-Konwalski, K. (2017). Single-nucleus Hi-C reveals unique
497 chromatin reorganization at oocyte-to-zygote transition. Nature *544*, 110-114.

498 Forsburg, S.L. (2003). Growth and manipulation of S. pombe. Current Protocols in Molecular
499 Biology, 13.16. 11-13.16. 17.

Gan, L., Ladinsky, M.S., and Jensen, G.J. (2013). Chromatin in a marine picoeukaryote is a disordered assemblage of nucleosomes. Chromosoma *122*, 377-386.

Gleizes, P.E., Noaillac-Depeyre, J., Leger-Silvestre, I., Teulieres, F., Dauxois, J.Y., Pommet, D., Azum-Gelade, M.C., and Gas, N. (2001). Ultrastructural localization of rRNA shows defective nuclear export of preribosomes in mutants of the Nup82p complex. The Journal of cell biology *155*, 923-936.

Harlen, K.M., and Churchman, L.S. (2017). The code and beyond: transcription regulation by the RNA polymerase II carboxy-terminal domain. Nature reviews Molecular cell biology *18*, 263-273.

Heumann, J.M. (2016). PEET (University of Colorado Boulder).

Heymann, J.B. (2001). Bsoft: image and molecular processing in electron microscopy. Journal of structural biology *133*, 156-169.

Hihara, S., Pack, C.G., Kaizu, K., Tani, T., Hanafusa, T., Nozaki, T., Takemoto, S., Yoshimi, T., Yokota, H., Imamoto, N.*, et al.* (2012). Local nucleosome dynamics facilitate chromatin accessibility in living mammalian cells. Cell reports *2*, 1645-1656.

Hirano, T. (2016). Condensin-Based Chromosome Organization from Bacteria to Vertebrates. Cell *164*, 847-857.

517 Hiraoka, Y., Toda, T., and Yanagida, M. (1984). The NDA3 gene of fission yeast encodes beta-
518 tubulin: a cold-sensitive nda3 mutation reversibly blocks spindle formation and chromosome
519 movement in mitosis. Cell *39*, 349-358.

520 Khoshouei, M., Radjainia, M., Baumeister, W., and Danev, R. (2017). Cryo-EM structure of
521 haemoglobin at 3.2 A determined with the Volta phase plate. Nature communications *8*, 16099.

522 Kimanius, D., Forsberg, B.O., Scheres, S.H., and Lindahl, E. (2016). Accelerated cryo-EM
523 structure determination with parallelisation using GPUs in RELION-2. Elife *5*.

524 Komarnitsky, P., Cho, E.J., and Buratowski, S. (2000). Different phosphorylated forms of RNA
525 polymerase II and associated mRNA processing factors during transcription. Genes &
526 development *14*, 2452-2460.

527 Kubik, S., Bruzzone, M.J., Jacquet, P., Falcone, J.L., Rougemont, J., and Shore, D. (2015).
528 Nucleosome Stability Distinguishes Two Different Promoter Types at All Protein-Coding Genes
529 in Yeast. Molecular cell *60*, 422-434.

530 Lantermann, A.B., Straub, T., Stralfors, A., Yuan, G.C., Ekwall, K., and Korber, P. (2010).
531 Schizosaccharomyces pombe genome-wide nucleosome mapping reveals positioning
532 mechanisms distinct from those of Saccharomyces cerevisiae. Nat Struct Mol Biol *17*, 251-257.

533 Luger, K., Mader, A.W., Richmond, R.K., Sargent, D.F., and Richmond, T.J. (1997). Crystal
534 structure of the nucleosome core particle at 2.8 A resolution. Nature *389*, 251-260.

535 Maeshima, K., and Eltsov, M. (2008). Packaging the genome: the structure of mitotic
536 chromosomes. J Biochem *143*, 145-153.

537 Martinez-Balbas, M.A., Dey, A., Rabindran, S.K., Ozato, K., and Wu, C. (1995). Displacement of
538 sequence-specific transcription factors from mitotic chromatin. Cell *83*, 29-38.

539 Mastronarde, D.N. (1997). Dual-axis tomography: an approach with alignment methods that
540 preserve resolution. Journal of structural biology *120*, 343-352.

541 McGinty, R.K., and Tan, S. (2015). Nucleosome structure and function. Chem Rev *115*, 2255-
542 2273.

543 Mizuguchi, T., Fudenberg, G., Mehta, S., Belton, J.M., Taneja, N., Folco, H.D., FitzGerald, P.,
544 Dekker, J., Mirny, L., Barrowman, J.*, et al.* (2014). Cohesin-dependent globules and
545 heterochromatin shape 3D genome architecture in S. pombe. Nature *516*, 432-435.

546 Nagano, T., Lubling, Y., Stevens, T.J., Schoenfelder, S., Yaffe, E., Dean, W., Laue, E.D.,
547 Tanay, A., and Fraser, P. (2013). Single-cell Hi-C reveals cell-to-cell variability in chromosome
548 structure. Nature *502*, 59-64.

549 Nagano, T., Lubling, Y., Varnai, C., Dudley, C., Leung, W., Baran, Y., Mendelson Cohen, N.,
550 Wingett, S., Fraser, P., and Tanay, A. (2017). Cell-cycle dynamics of chromosomal organization
551 at single-cell resolution. Nature *547*, 61-67.

552 Nozaki, T., Imai, R., Tanbo, M., Nagashima, R., Tamura, S., Tani, T., Joti, Y., Tomita, M.,
553 Hibino, K., Kanemaki, M.T., *et al.* (2017). Dynamic Organization of Chromatin Domains
554 Revealed by Super-Resolution Live-Cell Imaging. Molecular cell *67*, 282-293 e287.

555 Oesterreich, F.C., Herzel, L., Straube, K., Hujer, K., Howard, J., and Neugebauer, K.M. (2016).
556 Splicing of Nascent RNA Coincides with Intron Exit from RNA Polymerase II. Cell *165*, 372-381.

557 Oliva, A., Rosebrock, A., Ferrezuelo, F., Pyne, S., Chen, H., Skiena, S., Futcher, B., and
558 Leatherwood, J. (2005). The cell cycle-regulated genes of Schizosaccharomyces pombe. PLoS
559 Biol *3*, e225.

560 Ou, H.D., Phan, S., Deerinck, T.J., Thor, A., Ellisman, M.H., and O'Shea, C.C. (2017).
561 ChromEMT: Visualizing 3D chromatin structure and compaction in interphase and mitotic cells.
562 Science *357*.

563 Peng, X., Karuturi, R.K., Miller, L.D., Lin, K., Jia, Y., Kondu, P., Wang, L., Wong, L.S., Liu, E.T.,
564 Balasubramanian, M.K., *et al.* (2005). Identification of cell cycle-regulated genes in fission yeast.
565 Molecular biology of the cell *16*, 1026-1042.

566 Pettersen, E.F., Goddard, T.D., Huang, C.C., Couch, G.S., Greenblatt, D.M., Meng, E.C., and
567 Ferrin, T.E. (2004). UCSF Chimera--a visualization system for exploratory research and
568 analysis. J Comput Chem *25*, 1605-1612.

569 Pombo, A., and Dillon, N. (2015). Three-dimensional genome architecture: players and
570 mechanisms. Nature reviews Molecular cell biology *16*, 245-257.

571 Prescott, D.M., and Bender, M.A. (1962). Synthesis of RNA and protein during mitosis in
572 mammalian tissue culture cells. Exp Cell Res *26*, 260-268.

573 Rao, S.S., Huntley, M.H., Durand, N.C., Stamenova, E.K., Bochkov, I.D., Robinson, J.T.,
574 Sanborn, A.L., Machol, I., Omer, A.D., Lander, E.S.*, et al.* (2014). A 3D map of the human
575 genome at kilobase resolution reveals principles of chromatin looping. Cell *159*, 1665-1680.

576 Ricci, M.A., Manzo, C., Garcia-Parajo, M.F., Lakadamyali, M., and Cosma, M.P. (2015).
577 Chromatin fibers are formed by heterogeneous groups of nucleosomes in vivo. Cell *160*, 1145-
578 1158.

579 Robinow, C.F., and Hyams, J.S. (1989). General Cytology of Fission Yeasts. In Molecular
580 biology of the fission yeast, A. Nasim, P. Young, and B.F. Johnson, eds. (San Diego: Academic
581 Press), pp. 273-330.

582 Rustici, G., Mata, J., Kivinen, K., Lio, P., Penkett, C.J., Burns, G., Hayles, J., Brazma, A., Nurse,
583 P., and Bahler, J. (2004). Periodic gene expression program of the fission yeast cell cycle. Nat
584 Genet *36*, 809-817.

585 Scheres, S.H. (2012). RELION: implementation of a Bayesian approach to cryo-EM structure
586 determination. Journal of structural biology *180*, 519-530.

587 Struhl, K. (1998). Histone acetylation and transcriptional regulatory mechanisms. Genes &
588 development *12*, 599-606.

589 Taylor, J.H. (1960). Nucleic acid synthesis in relation to the cell division cycle. Ann N Y Acad Sci
590 *90*, 409-421.

591 Toda, T., Yamamoto, M., and Yanagida, M. (1981). Sequential alterations in the nuclear
592 chromatin region during mitosis of the fission yeast Schizosaccharomyces pombe: video
593 fluorescence microscopy of synchronously growing wild-type and cold-sensitive cdc mutants by
594 using a DNA-binding fluorescent probe. J Cell Sci *52*, 271-287.

595 Yakovlev, S., and Downing, K.H. (2011). Freezing in sealed capillaries for preparation of frozen
596 hydratedsections. J Microsc *244*, 235-247.

597 Yam, C., Gu, Y., and Oliferenko, S. (2013). Partitioning and remodeling of the
598 Schizosaccharomyces japonicus mitotic nucleus require chromosome tethers. Current biology :
599 CB *23*, 2303-2310.

600

601 **MAIN FIGURES**

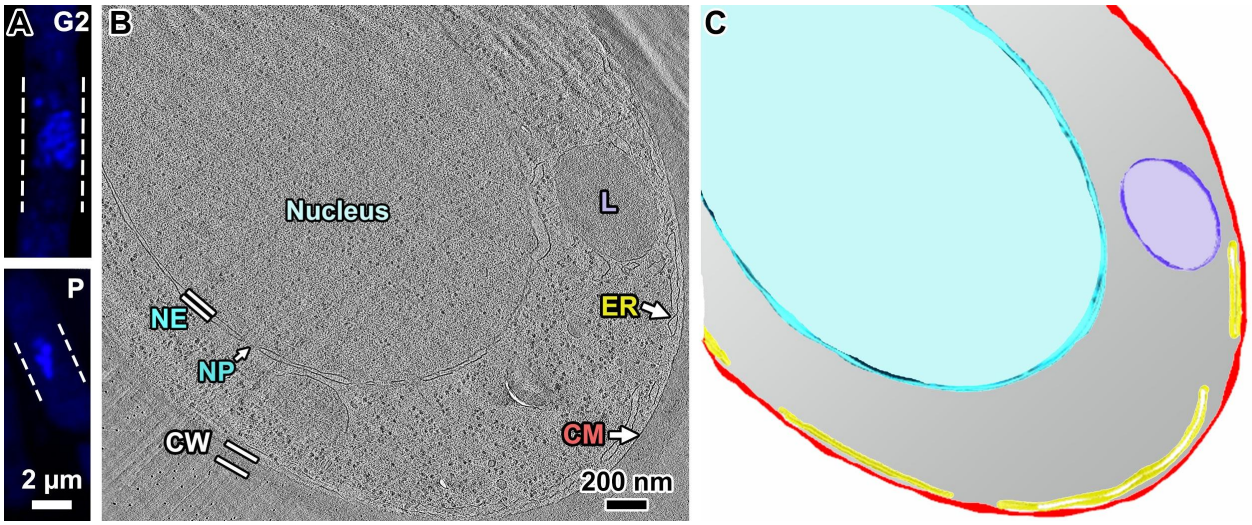

602

603 **Figure 1. Strategy to study chromosome condensation in *S. pombe*.**

604 (A) Fluorescence images of DAPI-stained G2-phase and prometaphase (P) cells.
605 Dashed lines indicate the cell boundaries. (B) Cryotomographic slice (25 nm) of a G2-
606 phase cell. NE: nuclear envelope; NP: nuclear pore complex; L: lipid body; ER:
607 endoplasmic reticulum; CM: cell membrane; CW: cell wall. The wavy features in the
608 upper portion of the cryotomogram are crevasses from sectioning; the thin parallel lines
609 running from 2 to 8 O'clock are knife marks. (C) Segmentation of the cryotomographic
610 slice in panel A, showing the cytological features with the same color scheme as the
611 text labels.

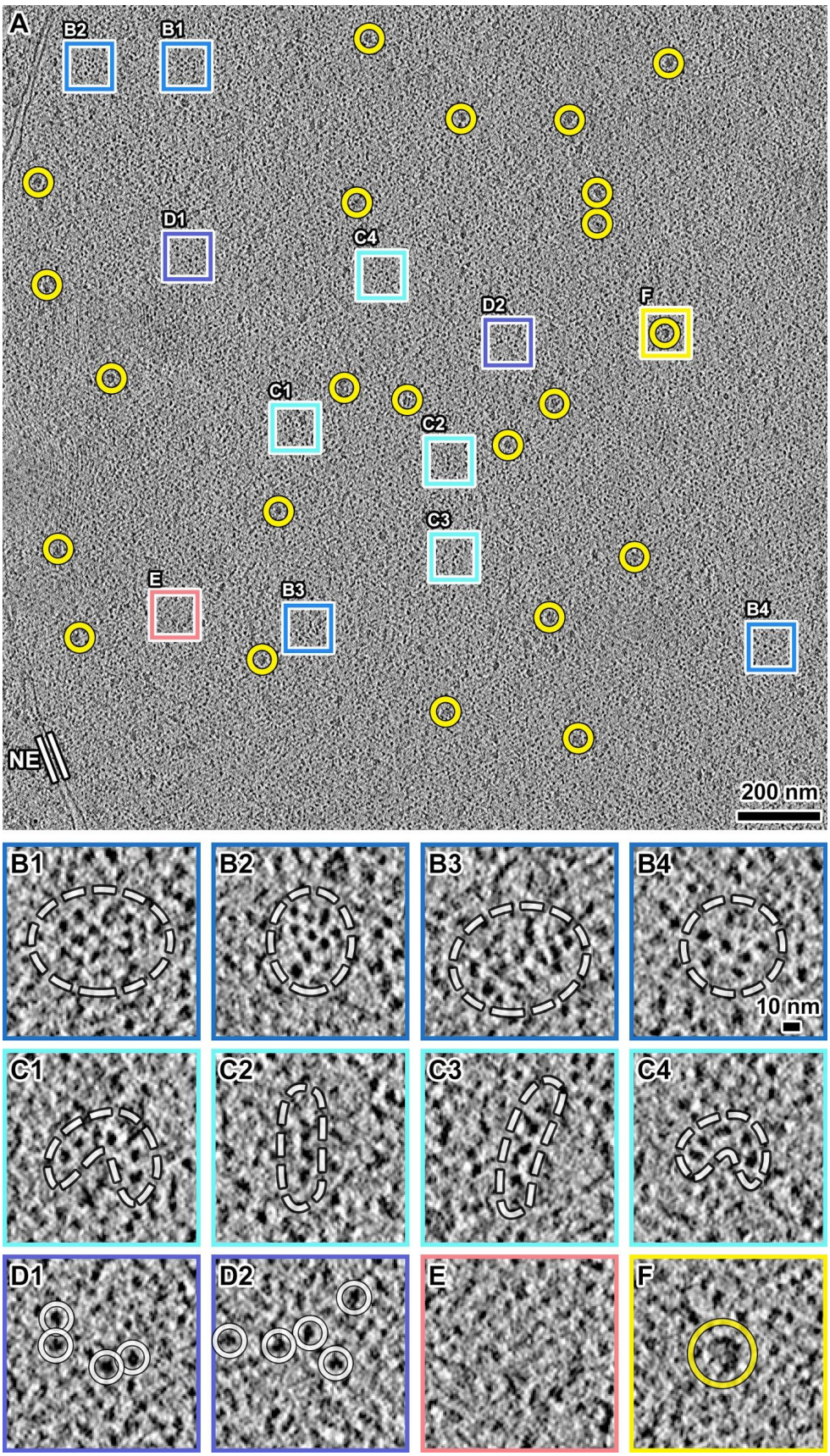

612

Figure 2. G2-phase chromatin consists of nucleosomes with heterogeneous packing motifs and dispersed megacomplexes.

(A) Cryotomographic slices (10 nm) of an interphase nucleus. Yellow circles: a subset of megacomplexes. (B1 - B4) Four examples of nucleosome clusters. (C1 - C4) Four examples of nucleosome chains. In panels B and C, the white dashed lines delineate the approximate boundaries of the nucleosome clusters. Due to their close packing and particulate nature, it is not possible to annotate the exact “outline” of a cluster. (D1 - D2) Two examples of loosely packed nucleosomes, which are circled. (E) An example position that has few nucleosomes. (F) An example megacomplex density.

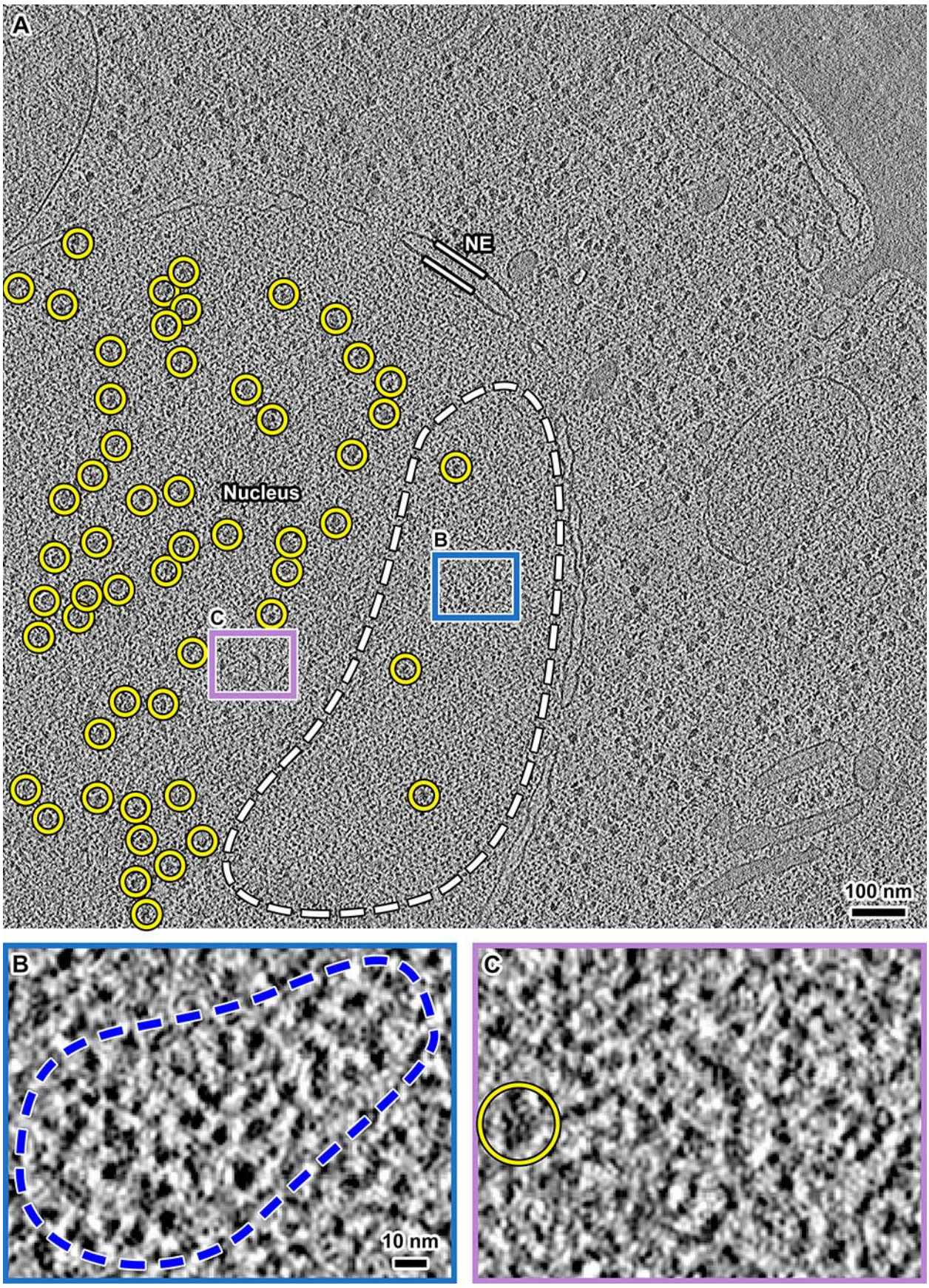

622

Figure 3. Condensed mitotic chromosomes contain few large molecular complexes.

(A) Cryotomographic slice (11 nm) of a prometaphase cell. NE: nuclear envelope. Yellow circles: megacomplexes. The position circled with dashed line is a condensed chromosome. Rectangular boxes are enlarged 6-fold in panels B and C. (B) An example position with many nucleosome-like densities forming a cluster, circled with a dashed blue line. (C) A representative position without nucleosome-like densities. Yellow circle: a megacomplex.

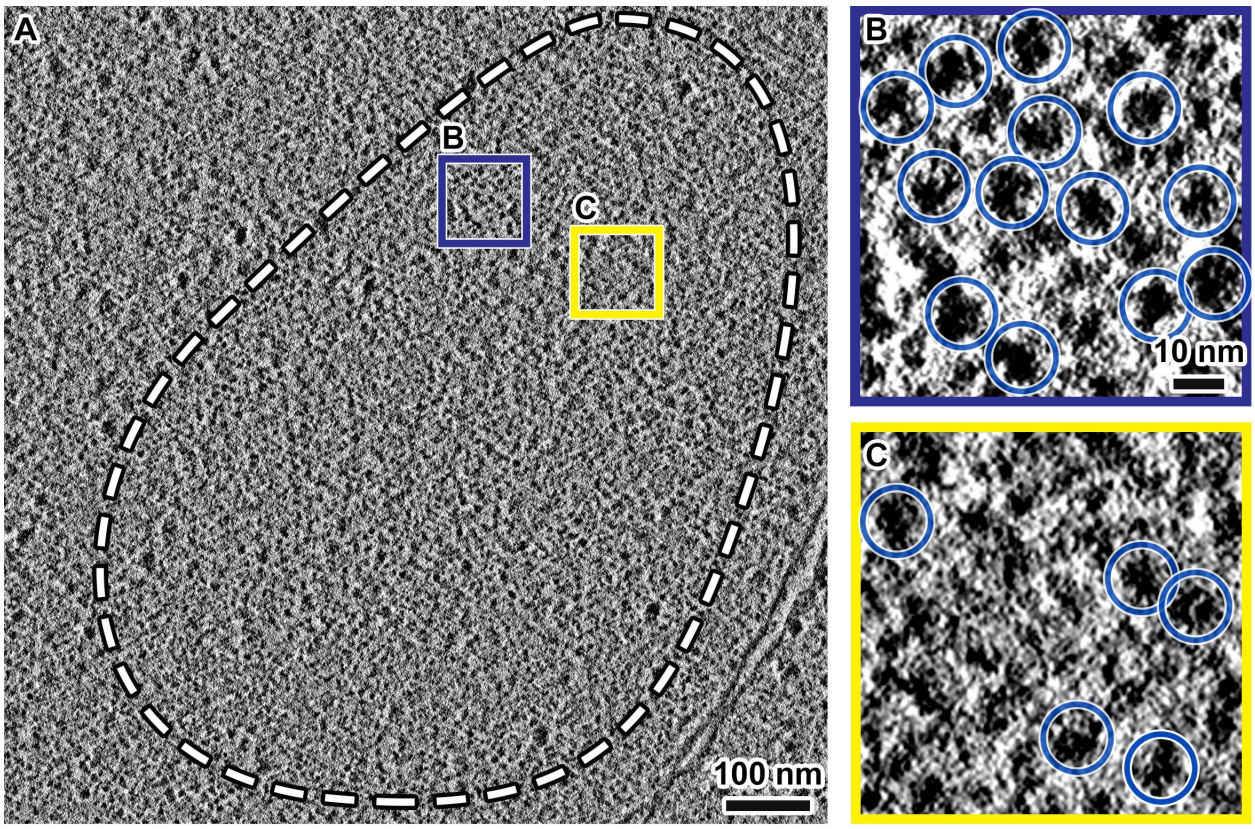

631

632 **Figure 4: Large nucleosome clusters and loosely packed nucleosomes coexist**

633 **within mitotic condensed chromosomes**

634 (A) cryotomographic slice (11 nm) of a nucleus in a prometaphase cell, imaged with

635 Volta phase contrast. White dashed line: approximate chromosome boundary, within

636 which there are fewer megacomplexes. (B) Five-fold enlargement of a position within

637 the mitotic chromosome that contains closely packed nucleosomes. (C) Five-fold

638 enlargement of a position within the mitotic chromosome that contains fewer

639 nucleosomes. Blue circles: nucleosomes.

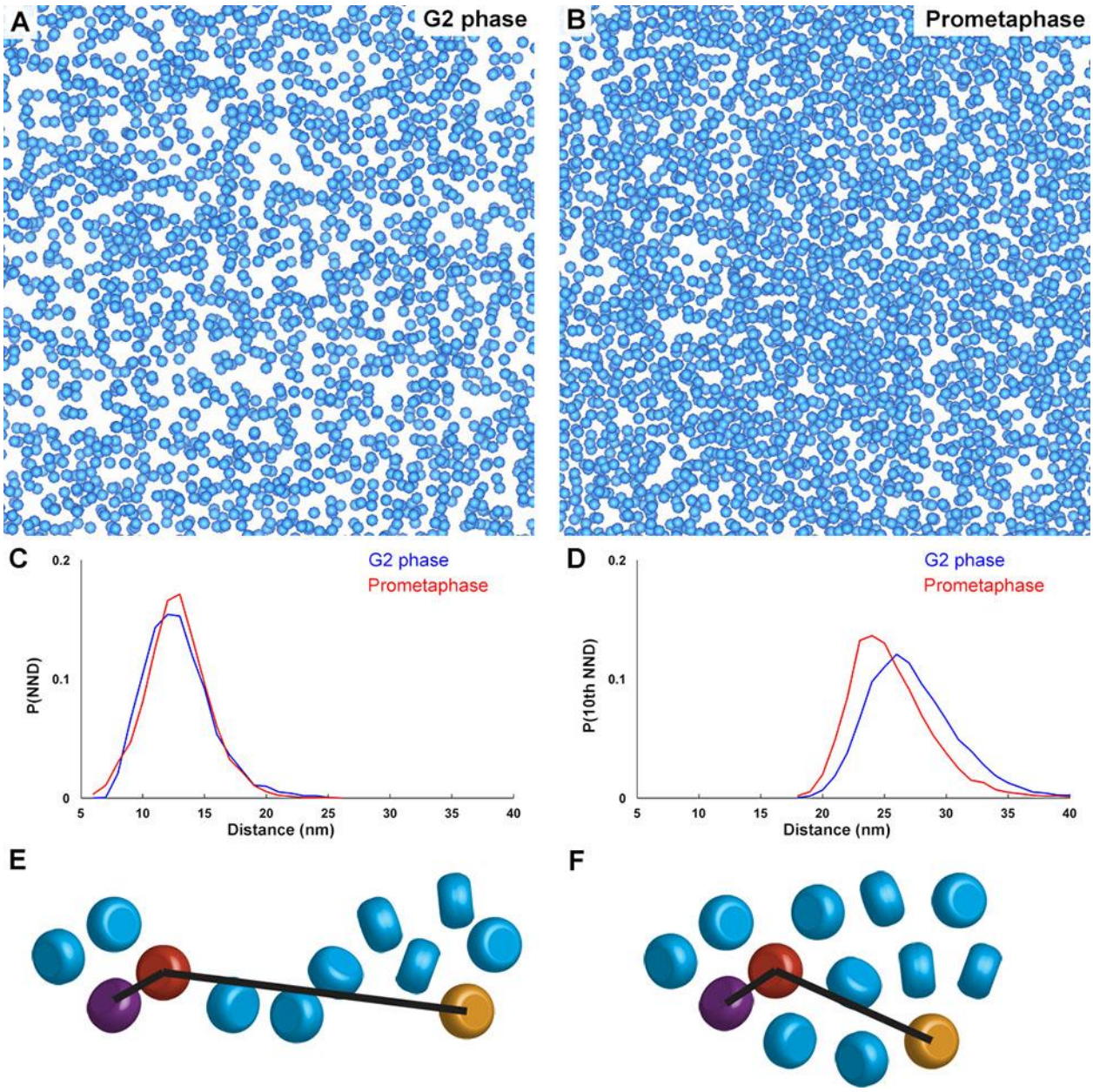

Figure 5: Prometaphase clusters grow larger but have constant local packing density.

(A and B) Template-matching hits of nucleosome positions (blue spheres) in Volta cryotomograms of (A) G2-phase and (B) prometaphase cells. (C) Nearest-neighbor distance (NND) analysis of template-matching hits. X-axis: NND, bin = 1 nm, Y-axis: normalized probability of each distance range. (D) Tenth NND analysis of template-

matching hits. The X- and Y- axes are the same as in panel C. (E, F) Cartoons showing how a small (E) and a large cluster (F) of nucleosomes (rounded cylinders) could have the same NND, but different 10^{th} NND. In each panel, the purple and orange nucleosomes are the respective nearest and 10^{th}-nearest neighbors of the red nucleosome.

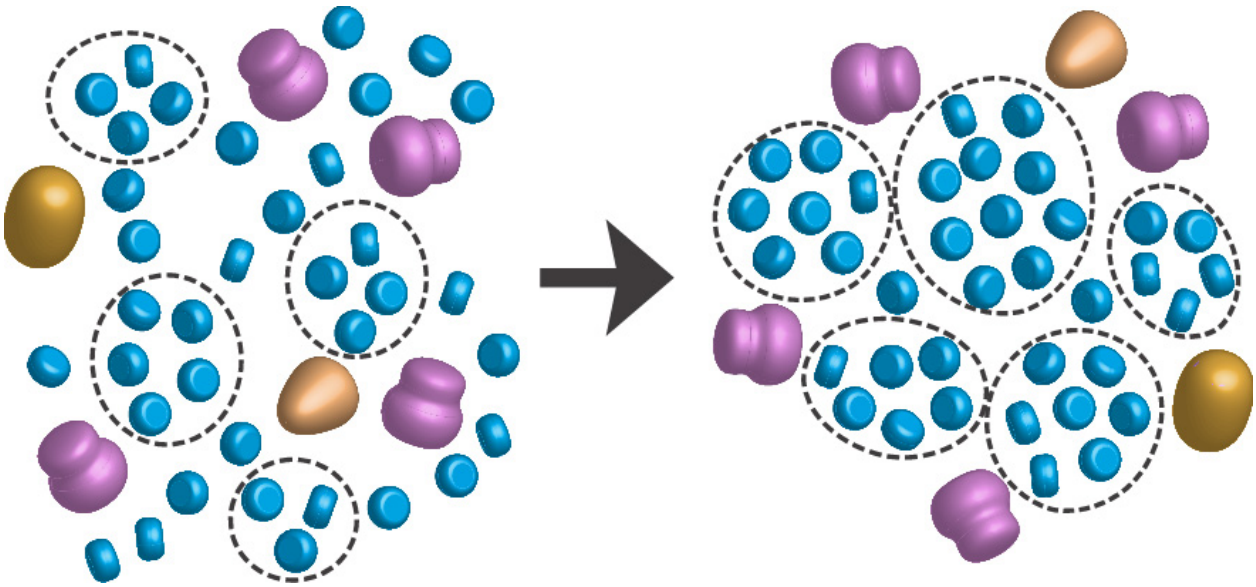

Figure 6: Model for mitotic chromosome condensation.

Interphase chromatin consists of both small nucleosome clusters and loosely packed nucleosomes. Blue: nucleosome; Gray: megacomplexes; dashed circles: nucleosome clusters. Note that this is a simplified model in which linker DNA is not shown. However, the absence of face-to-face interactions does reflect the results of 2-D classification. Megacomplexes (preribosomes, spliceosomes, transcription preinitiation complexes) are interspersed between the nucleosomes and nucleosome clusters. During mitotic chromosome condensation, most nucleosomes form larger clusters, thereby excluding or inhibiting the assembly of megacomplexes.